Coupled trace gas adsorption mechanisms within ESPs: promotion and inhibition of mercury removal

H.L. Clack

Department of Civil & Environmental Engineering, University of Michigan
1351 Beal Avenue, Ann Arbor, Michigan 48104 USA
Corresponding author: *hclack@umich.edu*

Keywords: Electrostatic Precipitator, Mercury, Powdered Activated Carbon

There is a large body of full-scale test results documenting powdered sorbent injection upstream of electrostatic precipitators (ESPs). These data generally provide overall mercury removal performance but lack the resolution and details needed to build understanding of the underlying mechanisms that drive simultaneous particle removal and trace pollutant adsorption. Clack and co-workers [2, 3] have analyzed material collected from ESP hoppers for carbon and mercury concentration variations during powdered activated carbon (PAC) injection tests. Concentrations of both generally increased from the front to the rear of the ESP as mean particle size concurrently decreased, suggesting that the fractionation of particle size and the associated size-dependent effect on electrostatic drift velocity and characteristic collection time influenced mercury adsorption. Following this trend, Clack [1] has numerically simulated the effect on total mercury adsorption (defined as the combined mercury adsorbed by both PAC particles suspended in the flue gas and the PAC content of the collected dustcake) of increasing PAC concentration in the collected dustcake. The results revealed that the two adsorption mechanisms are not additive, but rather competitive. Rather than augmenting total mercury adsorption and mercury removal efficiency, the PAC contained in the collected dustcake can actually *inhibit* mercury adsorption by the PAC particles within the boundary layer.

The present study expands on this counter-intuitive result by numerically simulating a range of mass transfer boundary conditions representing different PAC concentrations in the collected dustcake covering ESP collection electrodes. Details of this solution approach have been previously presented [1], and therefore are summarized here for brevity. Solved are the steady conservation equations for the electric field; the fluid flow field including electro-hydrodynamic forces; the charge-induced removal of polydisperse suspended solid particles from the flue gas; gas-particle mass transfer rates and reductions in gas-phase mercury concentration as particles are removed from the flue gas. The present analysis uses the operational conditions reported during full-scale PAC injection testing at AmerenUE's Meramec site [4], along with engineering drawings of the ESP involved. The computational domains represent a 3-wire 2×0.3 m (L×W) segment and a 9-wire 5×0.3 m segment of a complete ESP channel. The cylindrical (1 mm diameter, 0.5 m spacing) wire discharge electrodes are positioned along the channel centerline between the collection electrodes.

The electric field is assumed to depend only on the continuous phase fluid properties, and therefore can be solved independently of the fluid flow. For the solution of the electric parameters the spatial distribution of electric potential within the computational domain can be obtained numerically and independent of the fluid dynamic solution, subject to the specified material properties and applied boundary conditions. For a specified voltage applied to the discharge electrodes (–50 kV), a manual iteration scheme is used to obtain the space charge density distribution within the domain which produces, along with the computed electric field, the target value of current density (0.11 mA/m^2). Explicit simulation of the corona discharge is beyond the scope of the present study. The steady fluid flow field, including the effects of fluid-electric coupling, is governed by the Reynolds-averaged Navier-Stokes equations, modified to include an electric body force term. The native k-ε turbulence model and its default turbulence parameters are used without modification. Flue gas is approximated as air, incompressible, with property data extracted from the native materials database.

Only the PAC component of the suspended particles is considered for mercury adsorption, reflecting its much higher adsorption characteristics than most fly ashes. The initial PAC particle size distribution is log-normal, 1.5 μm < d_p < 150 μm with mean diameter of 20 μm and geometric standard deviation of 1.75, and the initial PAC particle concentration is 0.1 g/m^3, the equivalent of 6 lbs/MMacf (pounds of PAC per million actual cubic feet of flue gas), a relatively high rate of PAC usage based on current standards. The particle size distribution is divided into 11 size bins. Their spatial distributions of particle number density $ND_p(x,y,d_p)$ and particle volume fraction $\phi(x,y,d_p)$ are solved concurrently and in parallel in order to accurately render their collective effect on the spatial distribution of the gas-phase pollutant concentration $C(x,y)$, assumed here to be mercury. Once injected into the flue gas, PAC concentrations are sufficiently dilute as to make particle-particle interactions highly unlikely. Thus,

such interactions are not considered. Although the analysis incorporates one-way coupling between the fluid and the particle, two-way particle-fluid coupling is not considered. Gravitational acceleration is neglected.

The gas-particle mass transfer rate for particles of size d_p depends on their relative velocity with respect to the gas, or slip velocity. Thus, in considering in-flight adsorption of mercury within ESPs, gas-particle mass transfer is driven by size-dependent slip velocity, which in turn depends on electrostatic forces as determined by the spatially distributed electric field and space charge density. The inclusion in the present analysis of spatially varying particle slip velocity is a significant advance beyond the assumption of size-dependent but spatially uniform slip velocities employed in, e.g., the well-known Deutsch-Anderson equation, and our previous analyses [5-7].

Particle charging in an ESP is dominated by that occurring near the inlet, which in terms of time constants is small compared to the hydrodynamic or aerosol timescales typical of ESPs. A transient particle charging analysis following the method presented in Hinds [8] and applying the spatially averaged values of space charge density and electric field within the domain (1e–5 C/m^3 and 137,000 V/m, respectively) shows that after 1 second particles acquire 76% of their saturation charge in the 3-wire channel segment and 95% of their saturation charge in the 9-wire channel segment. For full-scale ESPs operating at similar, typical electrical conditions (–50 kV, 0.11 mA/m^2) and whose full-length channels contain dozens of discharge electrodes, the transient charging period would constitute an even smaller fraction of the hydraulic and aerosol timescales, reducing the error in assuming a constant particle charge throughout the domain equal to the saturation charge. The present analysis assigns a size-dependent saturation charge to the particles based on the spatially averaged mean values of electric field and space charge density. These super-micron particles are assumed to undergo solely field charging.

Assuming spherical particles, the Frössling equation [9] provides a correlation between the Sherwood number, a non-dimensional mass transfer parameter, and the particle Reynolds number based on slip velocity, as we have used previously [5-7]. The spatial distribution of mercury concentration C(x,y) [mol/m^3] in the domain is determined by the collective gas-particle mass transfer of PAC particles suspended in the flue gas (in-flight mechanism) and the mass transfer to the accumulated dustcake layer of collected particles on the collection electrodes (wall-bounded mechanism). For the wall-bounded mechanism, concentration boundary layers are calculated along with velocity boundary layers (including electric body forces), along the collection electrodes based on each assumed concentration of PAC in the dustcake.

Mercury removal efficiency in all cases is defined as the percentage difference between mercury rates of transport at the inlet and outlet of each channel segment. COMSOL Multiphysics™ (version 4.4) provided the computational platform as has been demonstrated previously in a similar applications [1, 10]. Computational times on a 64-bit HP Xeon workstation (2 2.93 GHz processors, 6 Gb RAM) are about 60 minutes for solving only the in-flight mechanism and about 225 minutes for solving the coupled in-flight and wall-bounded mechanisms for the 3-wire channel segment.

Previous numerical results [1] found that mercury adsorption by PAC in the collected dustcake produced a persistent mercury-depleted concentration boundary layer along the collection electrodes. The reduced gas-phase concentrations in turn reduced the driving potential for mercury adsorption by suspended PAC particles traversing this region before impacting the collection electrode. Figure 1 [1] illustrates this effect: Far from being additive, the two mercury removal mechanisms are competitive when coupled together ("coupled"), producing lower removal efficiencies than the suspended PAC particles alone ("in-flight"). Figure 1 also presents the variation of the ratio of the coupled mechanism removal efficiency to the in-flight mechanism removal efficiency. This ratio is slightly greater than unity nearest the inlet, decreasing to less than unity at the outlet, reflecting the growth of the concentration boundary layer and increasing inhibition of adsorption by the suspended PAC particles.

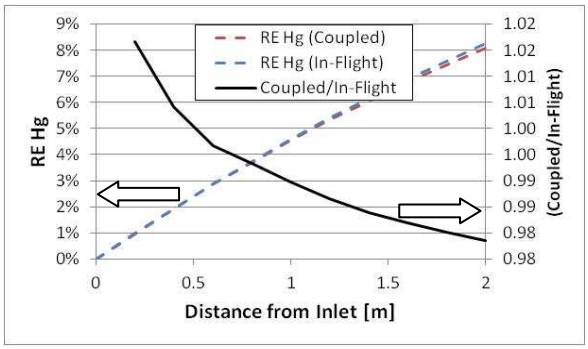

Figure 1. Simulation results from [1] of mercury removal efficiency in a 3-wire ESP channel segment resulting from adsorption by suspended PAC particles and adsorption to an accumulated dustcake containing 2.5% PAC. Dashed lines: Percent mercury removed as a function of distance from ESP channel inlet for (blue) in-flight only and (red) coupled in-flight and wall-bounded removal mechanisms. Solid line: Ratio of coupled removal efficiency to in-flight removal efficiency. Experimental conditions are as described in [1]

At nominal PAC injection rates less than 6 lbs/Mmacf, the result is a mixture of fly ash and PAC in the flue gas in which PAC concentrations are on the order of 2.5%. Disregarding differences between fly ash and PAC in particle size distributions, bulk densities, and dielectric constants, all of which would promote differences in their rates of collection, a first-order approximation would be to assume that

the collected dustcake over the collection electrodes in the first field of the ESP also reflects this 2.5% PAC concentration. However, subsequent fields and the hoppers beneath them are likely to be characterized by PAC enrichment due to PAC having smaller mean particle diameter and lower electrical resistivity that, respectively, delay particle collection and promote resuspension of collected particles. Collected field samples [2, 3] and laboratory testing [11] support this conclusion. Thus, the present analysis expands on the previous results by examining coupled mercury adsorption for conditions where the PAC concentrations in the collected dustcake exceed 2.5%.

Following the same approach used previously [1], PAC concentrations of 2.5%, 25%, 50%, 75%, and 100% were considered in the accumulated dustcake covering the collection electrodes of a 3-wire (2 m long) and a 9-wire (5 m long) ESP channel segment. The resulting removal efficiencies for in-flight alone, wall-bounded alone, and coupled in-flight and wall-bounded mercury removal mechanisms were determined from numerical simulation. For the 3-wire, 2 m long ESP channel segment, Figure 2 compares the computed wall-bounded, in-flight, and coupled mercury removal efficiencies that were obtained. From the figure it is apparent that regardless of the PAC concentration in the accumulated dustcake, the coupled wall-bounded and in-flight mercury removal efficiency always underperforms the sum of the two removal mechanisms considered separately.

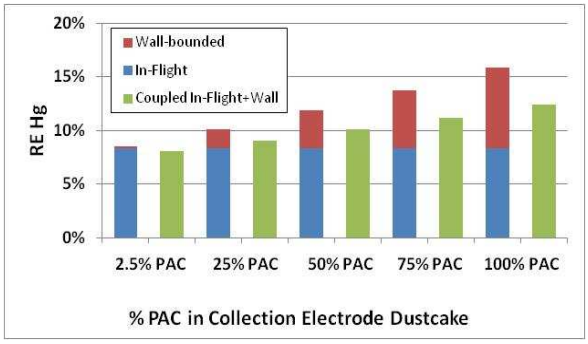

Figure 2. Computed values of mercury removal efficiency in a 3-wire, 2 m long ESP channel segment considering in-flight and wall-bounded removal mechanisms separately (blue, red) and coupled (green) for PAC concentrations in the dustcake layer of 2.5%, 25%, 50%, 75%, and 100%. Experimental conditions are as described in [1]

As the contribution of the wall-bounded mechanism increases with increasing PAC concentration in the dustcake, the performance deficit grows, from a fraction of a percentage point difference for 2.5% PAC in the dustcake to almost four percentage points for 100% PAC, an unlikely condition but one that is most relevant to the last mechanical field in an ESP. It should be noted that all mercury removal efficiency values are lower than those demonstrated in full-scale ESPs as a result of considering only segments of an ESP channel rather than an entire ESP channel that would be much longer and contain dozens of wire discharge electrodes.

As noted in the introduction, the virtual inability to interrogate the fluid-particle flows within a full-scale ESP leaves no options for obtaining experimental data that would provide insight into the mechanisms underlying simultaneous gaseous pollutant adsorption and particle removal within ESPs. These results illustrate the significance of the in-flight mechanism and how the wall-bounded mechanism is not only secondary to, but also competitive with, the in-flight mechanism in terms of total mercury removal efficiency.

References

[1] Clack, H.L., Aerosol and Air Quality Research, (2015), p. 2445-2455.

[2] Clack, H.L., Gorecki J., Macherzynski M., Golas J., Sherman L.S., Blum J.D., *Interpreting Mercury Capture within a Utility Electrostatic Precipitator through Analyses of Hopper-Segregated Fly Ash Samples* in *11th International Conference on Mercury as a Global Pollutant*. 2013: Edinburgh, Scotland.

[3] Hower J.C., Clack H.L., Hood M.M., Hopps S., Thomas G., International Journal of Coal Geology, (2016), p.

[4] Sjostrom, S., *Evaluation of Sorbent Injection for Mercury Control: Final Report for Sunflower Electric's Holcomb Station, AmerenUE's Meramec Station, American Electric Power's Conesville Station, DTE Energy's Monroe Power Plant, Missouri Basin Power Project's Laramie River Station and AmerenUE's Labadie Power Plant*. 2008, U.S. Department of Energy, National Energy Technology Laboratory.

[5] Clack H.L., Environmental Science & Technology, (2006), p. 3617-3622.

[6] Clack H.L., Journal of the Air & Waste Management Association, (2006), p. 759-766.

[7] Clack H.L., in *11th International Conference on Electrostatic Precipitation*. Hangzhou, China, 2009: Zhejiang University Press.

[8] Hinds W.C., *Aerosol Technology: Properties, Behavior, and Measurement of Airborne Particles*. 1999, New York: John Wiley & Sons.

[9] Frossling N., Beitr. Geophys., (1938), p. 170.

[10] Back A., Cramsky J., International Journal of Plasma Environmental Science & Technology, (2012), p. 33-42.

[11] Lee E.M., Clack H.L., Emission Control Science and Technology, (2015), p. 33-43.